Appl. Phys. B 71, 865–871 (2000) / Digital Object Identifier (DOI) 10.1007/s003400000412

Applied Physics B
Lasers
and Optics

Pressure dependence of vibrational Raman scattering of narrow-band, 248-nm, laser light by H_2, N_2, O_2, CO_2, CH_4, C_2H_6, and C_3H_8 as high as 97 bar

Y. Gu, Y. Zhou, H. Tang, E.W. Rothe*, G.P. Reck

Department of Chemical Engineering and Materials Science, Wayne State University, Detroit, MI 48202, USA
(Fax: +1-313/577-3810, E-mail: erothe@che.eng.wayne.edu)

Received: 23 December 1999/Revised version: 6 June 2000/Published online: 20 September 2000 –

Abstract. We have previously investigated methods that image high-pressure processes such as combustion inside automobile cylinders and aircraft engines, or chemical phenomena in supercritical fluids. Here we show that vibrational Raman scattering can simply obtain, quantitatively, densities of some combustion-relevant molecules. We use narrow-band KrF excimer-laser light. Measurements for H_2, N_2, O_2, CO_2, and CH_4 are in the pressure range from 1 to 60 bar, whereas those for C_2H_6 and C_3H_8 are up to their respective vapor pressures. All these species are at ambient temperature. Additional measurements are described for CO_2 up to 96.8 bar and 318 K, where CO_2 is a supercritical fluid. The O_2 measurements are complicated by a photochemical formation of O_3; those in supercritical CO_2 by drastic bending of the laser beam within this medium. We show that, for each gas, the Raman signal is directly proportional to gas density, thereby making *quantitative* analysis particularly convenient. For each species, we present an estimate of its Raman cross-section relative to that of N_2. However we recommend that future diagnostics users calibrate their own systems for relative species sensitivity.

PACS: 33.20; 82.40; 82.80

The development of some engineering applications, such as combustion in aircraft or automobile engines, or the uses of supercritical fluids, involves laser-based diagnostics of high-pressure media. Rothe and Andresen [1] have compared three light-scattering techniques for combustion analyses that use narrow-band KrF lasers. These are Rayleigh scattering, laser-induced fluorescence (LIF), and spontaneous Raman scattering.

Rayleigh scattering is far more intense than that from Raman. However it has the disadvantages that reflected and Mie light are difficult to separate from it; that the gas composition is needed in order to interpret the signal; and that it is not species specific.

*Corresponding author.

LIF analyses are state- and species-specific, and are sensitive, but they are difficult to interpret quantitatively because of the effect (a) of inelastic collisions in both the ground and excited states and (b) of laser parameters such as frequency stability, power fluctuations, and beam edge effects [2–6]. Such phenomena lead to signals that are often difficult to convert to species populations. Another possible high-pressure problem with LIF is broadening of the molecular spectral lines.

Raman scattering is much stronger in the UV than in the visible, because it increases as ν_i^4 (see below), where ν_i is the emitted frequency. In contrast to Rayleigh, Raman light can be separated from Mie light, and reflected light, by optical filters or a spectrometer. In contrast to LIF, we will show that Raman signals increase linearly with density; are, accordingly, larger at high pressure; and are easily calibrated.

Based on such considerations, Rothe and Andresen [1] concluded that the UV-Raman technique is best for the *quantitative* analysis of major mixture constituents when there is an adequate signal and it is sufficiently free of interfering emissions. These conditions are best met at the largest densities.

Narrow-band, tunable, KrF lasers have often been selected for Raman combustion work. The laser-beam's narrow bandwidth and tunability allow the use of wavelengths that avoid molecular excitations that produce interfering LIF. In most cases [1], users have obtained 1D images of temperature as well as of the density of all the major constituents. In combustion, these are typically N_2, O_2, CO_2, H_2O, and fuel. Alternatively, line-of-sight Raman in a backscatter mode can be used in which only two small windows are needed for optical access. At high pressures, 2D Raman images can also be obtained.

The main purpose of this work was to investigate whether the observed (i.e., within a detector solid angle Ω) Raman power I for a given species j is proportional to its density ϱ_j. The elementary theory of the Raman effect, for a collection of freely rotating molecules, suggests that this is a reasonable premise and we show here that it is correct. However, there was a concern: at greater densities, free rotation is more difficult and neighboring molecules may alter molecular polarizabilities.

Because some high-pressure gases deviate substantially from ideal-gas behavior, we use ϱ_j, rather than the pressure P, as the independent variable. If $I = c_j \varrho_j$, where c_j is a calibration constant for species j for a given apparatus, then Raman signals I can be directly converted into ϱ_j after c_j is determined. We do not examine the temperature T dependence of the signals here, but, at a fixed higher T, the dependence $I \propto \varrho_j$ should still apply. The calculation of the T-dependence of the signal at a fixed ϱ_j is much simpler than that for LIF, because Raman depends only upon molecular properties rather than collisional ones.

Surprisingly, it is difficult to determine from the literature whether $I \propto \varrho_j$ for various j. A number of points need to be considered. First, such data have usually been acquired with laser light at 488 or 514 nm, rather than the 248 nm used here. Second, some Raman lines narrow more with pressure than do others. Finally, there are typically peak shifts with pressure. The quantitative use of Raman at high pressure requires control of polarization and recognition that line positions and line widths [7–9] are dependent on pressure so that only the integrated intensity as a function of pressure is useful. However, the line-position shifts in our pressure range are negligible. For example, at 60 bar, the peak position for N_2 is shifted [7] from that near 0 bar (2328.14 cm^{-1}) by only 0.3 cm^{-1}. Our experimental resolution is about 25 cm^{-1}. For N_2, there is considerable line narrowing within our pressure range [9], but the integrated intensities are $\propto P$. Note that N_2 has nearly ideal gas behavior ($\varrho_{N_2} \propto P$, at a fixed T) within our range (see below) of T and P.

We use the term "high pressure" here only to contrast with near-atmospheric phenomena. In comparison to our maximum, $P = 96.8$ bar, Raman scattering has been reported from gases [10, 11] up to ≈ 3 kbar, and from solids [12] at ≈ 180 kbar.

After corrections for the non-ideal gas behavior, we found that the Raman differential cross section $d\sigma_j/d\Omega$ (see below) was, as hoped, a molecular parameter that was independent of pressure.

We investigated the species j = H_2, N_2, O_2, CO_2, CH_4, C_2H_6, and C_3H_8 at room temperature. Most measurements were in the range $P = 1$–60 bar. Exceptions were C_2H_6 and C_3H_8, whose upper limits were 40.5 and 10.1 bar, their respective vapor pressures at 25 °C. Another exception was CO_2, for which measurements were made under supercritical conditions as high as 317.7 K and 96.8 bar.

We measured the pressure dependence of the Raman power I. We then converted the measured P to the corresponding ϱ_j by means virial coefficients that are listed in Table 1, and, for supercritical CO_2, with a more elaborate equation of state. We also found individual cross sections $d\sigma_j/d\Omega$ relative to $d\sigma_{N_2}/d\Omega$. Our normal 60-bar upper limit was arbitrarily established from the maximum operating pressure of an aircraft engine to which Raman diagnostics were subsequently applied and by the linear range (see below) of our selected pressure transducer. The one-bar lower limit occurred mainly because of lack of precision of that pressure transducer (see below), but also because of the larger measurement errors for the smaller Raman signals. In order to interpret Raman data conveniently, the value of the $d\sigma_j/d\Omega$ (see below) must be independent of pressure.

1 Vibrational Raman scattering

Vibrational Raman scattering is routinely used [13] to deduce molecular structure and to perform chemical analysis. When a laser with a frequency ν_{laser} interacts with molecules, a Stokes–Raman spectrum of the scattered light is observed at frequencies ν_i that are given by

$$\nu_i = \nu_{laser} - \nu_{molec} \tag{1}$$

where each frequency ν_{molec} is that of a vibrational mode i in a molecule [14]. Raman intensities at selected ν_i are expected to yield populations of the corresponding molecular species.

A laser beam has an electric field vector $\boldsymbol{E}_0$ and an intensity I_0 (for example, in W/m^2). Then $I_0 \propto E_0^2$, where E_0 is the amplitude. It can be shown [13] that for linear Raman scattering from one molecule, the amplitude of the induced dipole moment is $\propto E_0$. The total Raman power I_T (for example, in W) that is radiated by that dipole at frequency ν_i into the entire solid angle, (i.e., into $\Omega = 4\pi$) is $\propto E_0^2$. Thus the ratio I_T/I_0 is independent of I_0 and is the total Raman cross section σ_j (for example, in m^2). A physical interpretation is that molecule j with cross section σ_j will Raman-scatter (into ν_i) all light incident upon an area equal to σ_j. Observation is usually in a given direction with some limited range of solid angle, Ω. Thus the differential cross section $d\sigma_j/d\Omega$ (for example, in m^2/sr) is more useful here.

We use a common experimental arrangement. It includes a laser beam that is nearly-linearly polarized along $\boldsymbol{E}_0$ and a detector that receives Raman light in a direction perpendicular to $\boldsymbol{E}_0$ but that has no polarization analyzer for the scattered light. Let the laser beam propagate along the y axis. We observe the scattered light along the x axis. The electric vector $\boldsymbol{E}_0$ is parallel to the z axis. That choice of $\boldsymbol{E}_0$ maximizes the Raman signal for diatomic species.

Table 1. Virial coefficients from [19] and values for Z_i calculated from these coefficients at 298.15 K using (3)

Gas	B cm^3/mole	C cm^6/mole	Z_i 1 bar	Z_i 10 bar	Z_i 20 bar	Z_i 60 bar
H_2	−14.37	356	0.9994	0.9942	0.9885	0.9661
N_2	−4.71	1315	0.9998	0.9983	0.9970	0.9962
O_2	−16.24	1163	0.9994	0.9936	0.9875	0.9660
CO_2	−120.5	4350	0.9951	0.9497	0.8962	0.6488
CH_4	−42.7	2450	0.9983	0.9829	0.9660	0.9003
C_2H_6	−185.8	10 600	0.9925	0.9212	0.8345	
C_3H_8	−333	−65 000	0.9863	0.8371		

For this setup, the differential cross-section is given by Long [13] as

$$\mathrm{d}\sigma_\mathrm{j}/\mathrm{d}\Omega = C\nu_\mathrm{i}^4 g_\mathrm{i}[(a_\mathrm{i})^2 + (7/45)(\gamma_\mathrm{i})^2]/\{[\nu_\mathrm{molec}] \times [1-\exp(-h\nu_\mathrm{i}/kT)]\}\,, \quad (2)$$

where C is a collection of apparatus and molecule-independent physical constants. For each vibration i, g_i is the degeneracy, and a_i and γ_i are the mean values and the anisotropy of the derived polarizability tensor. Because of resonance effects, (2) applies best when the value of ν_laser is far from that of ν_molec. Because absolute cross sections are difficult to measure, we report $\mathrm{d}\sigma_\mathrm{j}/\mathrm{d}\Omega$ relative to that of N_2.

Equation 2 shows that $\mathrm{d}\sigma_\mathrm{j}/\mathrm{d}\Omega$ with UV light is much larger than that with visible light because it varies as ν_i^4, and $\nu_\mathrm{i} \approx \nu_\mathrm{laser}$. Equation (2) also includes the temperature dependence of the cross section. Although it does not appreciably affect our 25–44 °C data, (i.e., $1-\exp(-h\nu_\mathrm{i}/kT) \approx 1$), it must be considered at high T.

2 Experimental

We modified a Lambda Physik Model EMG150-EST laser to have a "single-pass" configuration. Most of those modifications were described elsewhere [15]. They serve to increase both the fraction of the beam that is narrow band and the degree of linear polarization. The laser light has $\approx$ 1-cm^{-1} bandwidth, has a $\approx$ 13-ns pulse length, a $\approx$ 1-mrad divergence, and can be tuned between about 247.8 to 248.8 nm. The pulse energies are in the range 150–225 mJ and the repetition rate was $\approx$ 3 Hz. A polarizer cube and half-wave plate are located between the laser's oscillator and amplifier. The cube maximizes the degree of linear polarization and the plate allows us to adjust the direction of $\boldsymbol{E}_0$. The degree of linear polarization is $> 95\%$, as measured by the ratio of Rayleigh signals (from argon) when $\boldsymbol{E}_0$ is set to be (a) in its normal direction, and (b) when perpendicular to it.

The laser beam passes through a cell that contains the sample. We collect Raman light that is emitted in a direction perpendicular to both the laser beam path and to $\boldsymbol{E}_0$. The light is dispersed in, and measured by, an imaging spectrograph.

Figure 1 is an apparatus schematic. We reduce the laser beam's cross section to be about 0.5×1 mm by means of a spherical lens L3. The cell's main bore has a 12.7-mm diameter and a 127-mm length. The cell is normally at room temperature, but with supercritical CO_2, it is maintained near 40 °C by means of an air bath. The laser beam travels along the cylindrical axis and the Raman light exits through another 12.7-mm hole bored in the middle of the cell. The three ports have Suprasil 2 windows. The scattered light is gathered with a 38-mm-diameter lens L1 that is located about 200 mm from the cell, i.e., $\Omega = 0.028$ sr. Spherical lenses L1 and L2 focus it through the entrance slit of an imaging spectrometer. An image of the 12.7-mm-long sample is projected onto the slit and a spatially-resolved (1-D) spectrum is initially recorded. Because the gas is homogenous along the laser beam, we integrate over a center portion of the 1-D image. We ignore about 10% at each end in order avoid possible edge effects. The integrated intensity over that selected spatial region yields a single value for each gas and pressure.

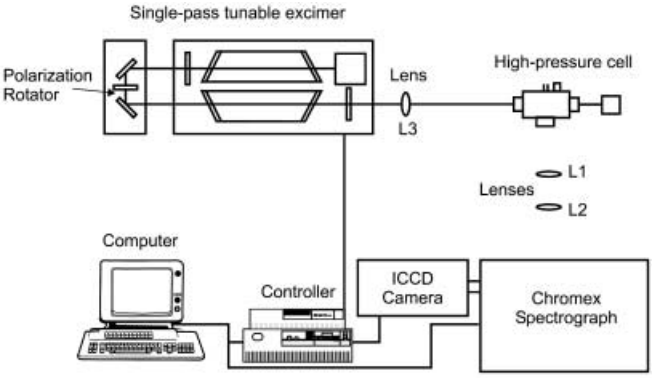

Fig. 1. Schematic of the spectrally resolved 1-D imaging system

We measure P with an Entran transducer (EPX-V01-70B), whose nominal range is $P = 0$–70 bar. According to the manufacturer, within this range, the transducer's combined linearity and hysteresis errors are $\Delta P = \pm 0.35$ bar. That leads to large fractional errors ($\Delta P/P$) at the lowest pressures. For supercritical CO_2, we use an analogous transducer (EPX-V-01-150B) with a range $P = 0$–150 bar.

Our imaging spectrograph is a 1/4-m Chromex Model 250IS. Its ruled grating has 2400 grooves per mm and it is blazed for 250 nm. The light is transmitted by the spectrograph to a Princeton Instruments intensified CCD camera (Model ICCD-576G/RB) that is located on the spectrograph's exit plane. The images are processed with Princeton Instruments' CSMA software.

We adjust the spectrograph's slit width so as to have a spectral resolution of about 25 cm^{-1}. Then each diatomic molecule yields a resolved single Raman peak at the wavenumber values listed in Table 2. For both CO_2 and CH_4, we sum the intensities for the two normal modes listed in Table 2. These peaks are from Fermi resonances [14]. For ethane [16] and propane [17, 18] the Raman spectra are more complex, and we sum the intensities from a region between about 2700 to 3200 cm^{-1}, which is mainly caused by the C−H stretch mode.

For measurements of the pressure dependence of I, for a single species j, we apply a peak-measuring program within CSMA to find the areas of each spectral peak. We first select a point on the base line on each side of the peak. Then the program draws a straight line between those points and finds the area that lies between that line and the peak. This works for a single species, because the peak shapes from different densities are geometrically similar.

We initially also tried CSMA to measure intensities from different species relative to those from nitrogen. That was more difficult because the simple N_2 peak shape is very different from those of the more complex CO_2, C_2H_6, and C_3H_8. Accordingly we use a more sophisticated peak-fitting program (*PeakFit* by Jandel Scientific) to determine all areas used in comparing different species.

3 Procedure

We set the camera's intensifier gate to be 100 ns. That is short enough to suppress all cw light, but long enough to avoid problems caused by jitter. Each Raman spectrum is the sum of

Table 2. Room-temperature Raman differential cross sections relative to those for nitrogen: i.e., $d\sigma_j/d\Omega/d\sigma_{N_2}/d\Omega$. For CO_2 our total includes more than the two cited peaks. No supercritical data is included here. Note that differences in laser polarization and in detection angle make precise comparison between different experimental arrangements difficult

Gas	Wavenumber (cm^{-1}), modes	Scaled from 337 nm[a]	Burris 282 nm[b]	Koba-yashi 248 nm[c]	Bischel 248 nm[d]	Schrötter various[e]	Our data 248 nm
H_2	4160	2.9			3.12	4.2	4.8 ± 0.3
N_2	2331	$\equiv 1.00$	$\equiv 1.00$	$\equiv 1.00$	$\equiv 1.00$	$\equiv 1.00$	$\equiv 1.00$
O_2	1556	1.2	2.1 ± 0.3	2.5	2.57	1.1	1.7 ± 0.1
CO_2	1388, ν_1	1.3		1.9		1.11	0.8 ± 0.2
CO_2	1285, $2\nu_2$	0.9		1.2		0.75	0.4 ± 0.2
CO_2	Total	2.2		3.1			1.33 ± 0.04
CH_4	2914; ν_1	7.2	8.4 ± 0.4		7.23	8	11 ± 1
CH_4	3022, ν_3	4.5		8.4			
CH_4	Total	11.7		11.7			19 ± 0.4
C_2H_6	2899, 2955	27					28 ± 1
C_3H_8	2903, 2920, 2946, 2967					32	42 ± 1

[a] A.C. Eckbreth: *Laser Diagnostics for Combustion Temperature and Species*, 2nd edition (Gordon and Breach Publishers, Amsterdam 1996) p. 222
[b] J. Burris, T.J. McGee, W. Heaps: Appl. Spectrosc. **46**, 1076 (1992)
[c] T. Kobayashi, M. Konishi, M. Ohtaka, S. Taki, M. Ueda, K. Kagawa, H. Inaba: In *Laser Diagnostics and Modeling of Combustion*, ed. by K. Iinuma, T. Asanuma, T. Ohsawa, J. Doi (Springer, Berlin, Heidelberg 1987) Chapt. 5.4. They used an unpolarized broadband excimer without polarization analysis of the Raman light
[d] W.K. Bischel, G. Black: Excimer Lasers-1983, AIP Conference Proc. 100, ed. by C.K. Rhodes, H. Egger, H. Pummer (American Institute of Physics, New York 1983) pp. 181–187
[e] see [24]

intensities from 100 laser-shots. Background is similarly acquired with the laser off and is subtracted from the signals. At one bar, the Raman intensities are smallest so that their relative errors are the largest. As the pressure P is increased, intensities become stronger and there is less error. As previously discussed, the precision of $\Delta P/P$ is also poorest at the lowest P.

We describe below two different procedures. The first is to measure the signal dependence upon density for a particular gas and the second is to obtain the ratio of signals from different gases.

In order to find whether $I \propto \varrho_j$ for each j, we obtain data at steadily increasing pressures. We wait for about two minutes after each pressure change in order to have a quiescent gas and to minimize any resulting temperature changes. For each species we optimize the system settings, including the camera gain.

In order to find the cross sections $d\sigma_j/d\Omega$ of species j relative to N_2, we interchange N_2 and gas j at each of a large set of pressures P. These quick interchanges minimize the effect of parameter changes, such as those caused by aging excimer gas. At any value of P, $\varrho_{N_2} \neq \varrho_j$ because the gases are not ideal. In order to compare at $\varrho_{N_2} = \varrho_j$, we converted our N_2 data, $I(P)$ to $I(\varrho_{N_2})$ by means of the virial equation and fitted these to obtain analytical functions for $I(\varrho_{N_2})$. Then we could calculate the relative cross sections.

In both procedures, we calculate the densities ϱ_j, from the measured pressures via the truncated virial expansion

$$PV_j = (1 + B_j/V_j + C_j/V_j^2)RT \; . \tag{3}$$

where V_j is the molar volume, R is the universal gas constant, and B_j and C_j are recommended [19] virial coefficients (listed in Table 1) for species j. The quantity inside the parentheses is the compressibility, Z_j, which is $PV_j/RT \equiv 1.0$ for an ideal gas. In our pressure range, at 25 °C, N_2 has nearly ideal-gas behavior, for example, $Z_{N_2} = 0.9998$ and 0.996 at 1 and 60 bar, respectively. In contrast, CO_2 has significant deviations: for example, $Z_{CO_2} = 0.64$ at 60 bar. Because the Raman intensity is expected to depend upon the molar density $\varrho_j (= 1/V_j)$, we can find that

$$\varrho_j = [RT/P + B_j + (C_j - B_j^2)P/RT]^{-1} \; . \tag{4}$$

Figures 3–5 show plots of Raman intensity I vs. ϱ_j. In Figs. 3 and 4, ϱ_j was calculated with (4), whereas ϱ_{CO2} for Fig. 5 was calculated as described below.

4 Experimental anomalies

Our experiments would seem to be straightforward, but we had two serious complications. With O_2, and with supercritical CO_2, the laser beam failed to pass through the cell, even though O_2 and CO_2 are both transparent at 248 nm. The causes were different for the two molecules. Each was interesting, and they illustrate, once again, that even a conceptually simple experiment can yield unexpected events.

4.1 Photochemistry with oxygen

We usually Raman-scattered from a static gas. Oxygen could not be successfully measured that way. The first few laser pulses yielded normal results, but then the laser beam became so attenuated that neither Raman light nor transmitted laser light emerged from the cell. This was caused by O_3, which strongly absorbs at 248-nm. Slanger et al. described such ozone formation [20] as a result of 248-nm irradiation of O_2. That was surprising because the low-energy threshold for the photodissociation of O_2 is 242.4 nm. The mechanism is still not clear, although several have been suggested [21].

In order to minimize the O_3 density, we maintained a gas-flow through the cell. That led to normal responses (see Fig. 2) except at $P > \approx 50$ bar. Because many diagnostic applications do not involve static gas, Raman analyses of O_2 should work for these.

4.2 Beam deflection in supercritical carbon dioxide

When we increased the density of CO_2, ϱ, at $T = 40\,^{\circ}\mathrm{C}$, the Raman signal I initially increased correspondingly. However, surprisingly, with a further increase in ϱ, it reached a maximum and then steadily decreased.

This occurred because the laser beam bent downward in supercritical CO_2 and the *deflection was so large* that the laser beam failed to reach either the Raman observation region or the cell's exit window. The beam deflected because the CO_2 had a negative gradient of its refractive index, $\mathrm{d}n/\mathrm{d}z$, where z is the vertical coordinate. That gradient was caused by a positive temperature-gradient $\mathrm{d}T/\mathrm{d}z$.

The cell's bottom was about 1.5 °C cooler than the other sides. Thus the CO_2 density increased with depth, i.e., $\mathrm{d}\varrho/\mathrm{d}z < 0$ and that stabilized the supercritical fluid against convection. Because carbon dioxide has a high compressibility near its critical point ($T_c = 304.2$ K, $P_c = 73.8$ bar), $|\,\mathrm{d}\varrho/\mathrm{d}z\,|$ is large. We calculated $\mathrm{d}\varrho/\mathrm{dT}$ from the Wagner–Span equation of state [22] for CO_2, and combined it with $\mathrm{d}T/\mathrm{d}z$ in order to get $\mathrm{d}\varrho/\mathrm{d}z$. Next we relate n to ϱ, so that we can obtain $\mathrm{d}n/\mathrm{d}z$. The specific refraction r for CO_2, at 248 nm is [23]

$$r \equiv [(n^2-1)/(n^2+2)]/\varrho = 1.66 \times 10^{-4}\,\mathrm{m^3\,kg^{-1}}\,. \qquad (5)$$

Equation 5 indicates that n will increase with ϱ so that $\mathrm{d}n/\mathrm{d}z$ is negative in our setup. We did a sample calculation for a pressure of 90 bar, and in a temperature range from 312–313 K. We found that $(\partial n/\partial T)_P = -0.0115 \pm 0.0005\,\mathrm{K^{-1}}$. That is about 20 times larger than that for a typical liquid and occurs because of the large compressibility of supercritical CO_2. The bending is caused by the same effect (Fermat's principle) as the appearance of mirages caused by hot surfaces.

Once this cause was established, we reduced $\mathrm{d}T/\mathrm{d}z$ sufficiently to obtain a linear dependence of I upon ϱ. We had to be careful because active convection occurs when $\mathrm{d}T/\mathrm{d}z$ is near zero or negative, and that scatters the laser beam.

5 Results

The relative differential cross sections $(\mathrm{d}\sigma_j/\mathrm{d}\Omega)/(\mathrm{d}\sigma_{N_2}/\mathrm{d}\Omega)$, as a function of density, are shown in Fig. 2. As expected, they are independent of density. Averaged values are shown in Table 2, along with errors based on repeatability. These error bars are reasonable and this implies that such Raman analyses can be quite accurate. The N_2 data are very smooth and the scatter in the relative cross sections shown in Fig. 2 are mainly caused by those for species other than N_2.

Table 2 shows substantial disagreement with the results of other investigators. That is not surprising. They used different arrangements than ours. Some important parameters include laser wavelengths, laser or detector polarization setups, detection solid angles, spectrometers, camera sensitivities, etc. The ν_i^4 scaling in (2) need not be correct in the vicinity of resonances. An equation [13] analogous to (2) applies when the electric vector of the laser light $\boldsymbol{E}_0$ is turned by 90° from that assumed there and it yields quite different results. For example, the results of Kobayashi et al., which are listed in Table 2, employed the same wavelength as ours, but had a different polarization setup. Similar statements apply to measurements made with either intentional polarization analysis of the Raman light or intrinsic polarization-discrimination in the measuring device. Most lasers have a distribution of $\boldsymbol{E}_0$ direction.

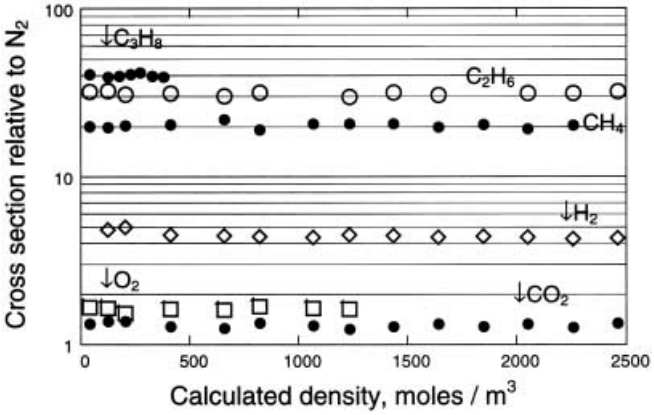

Fig. 2. Measured values of $\mathrm{d}\sigma_j/\mathrm{d}\Omega/\mathrm{d}\sigma_{N_2}/\mathrm{d}\Omega$ i.e., t e differential Raman cross sections, relative to that of N_2, obtained at various densities at 25°C

It is difficult to imagine a source of a large random laboratory error in any of the cross sections relative to N_2 measured by the various investigators. That is because such experiments consist solely of interchanging N_2 and the gas to be measured, finding the density, and observing the resulting intensity ratios.

Schrötter and Glöckner [24] present a detailed discussion of such points and they also present a table of their measurements, as well as those of others. That table also shows agreement for some species, and disagreement with others.

If the divergence among the results listed in Table 2 is too large for potential users of Raman diagnostics, we recommend that they calibrate their own apparatus (see next section) rather than to rely on literature values.

Figures 3 and 4 are representative plots of observed signal I versus room-temperature density ϱ_j. We made several replicate runs for each species and obtained similar results. The signals for each gas were acquired at a particular laser intensity I_0 and camera gain. Thus raw Raman signals from different species j are not directly comparable. In Figs. 3 and 4, we have adjusted the otherwise arbitrary slopes to be proportional to the ratios of relative cross sections that were separately determined and that are listed in Table 2. As was discussed above, measurements at small P have larger relative errors because (a) the signals are smallest there and (b) the pressure transducer has a constant error $\Delta P = \pm 0.35$ bar throughout our 1–60 bar range.

Figures 3 and 4 demonstrate that the Raman signal is a linear function of ϱ_j and that it may be used as a direct measure for ϱ_j. Figure 5 shows that this linearity is maintained at the still-larger densities existing in the supercritical CO_2. *The linearity displayed in Figs. 3–5 is our main point.*

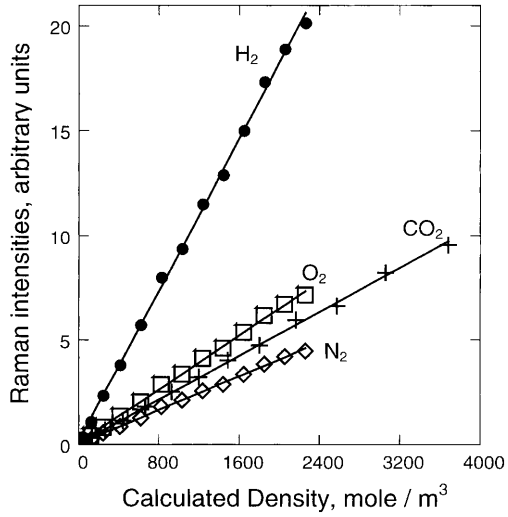

Fig. 3. Plot of scattering intensity vs. molar density for a representative data set for hydrogen, oxygen, carbon dioxide, and nitrogen, and a least-squares linear fit to each. Each slope has been adjusted to be proportional to its relative differential cross section (See Table 2). All species are at ambient temperature and the maximum densities correspond to about 60 bar

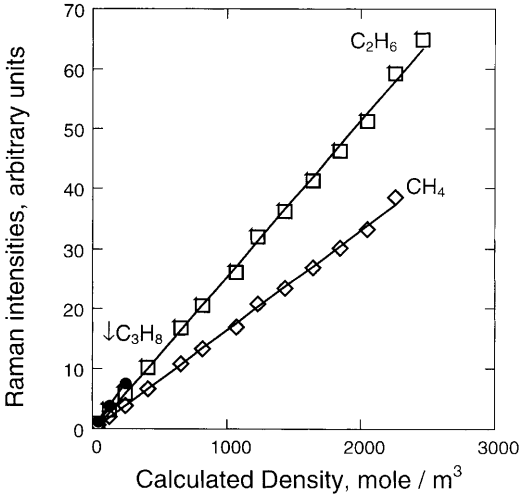

Fig. 4. Plot of scattering intensity vs. molar density for a representative data set for propane, ethane, and methane, and a least-squares linear fit to each. Each slope has been adjusted to be proportional to its relative differential cross section (See Table 2). All species are at ambient temperature. The small range of propane data (*black circles*) is caused by its comparatively low vapor pressure

6 Conclusions

[1] contains a detailed comparison of various excimer-laser-based diagnostics. Our work reinforces the conclusion that Raman scattering of 248-nm light is very well suited for diagnostics at high pressures. Although there is sometimes interference from fluorescence, this can often be nearly eliminated by appropriate polarization techniques or laser tuning. For example, Grünefeld et al. [25], analyzed an oil burner and an IC engine. Their laser and analysis system were similar to ours. They captured light emitted at two orthogonal polarizations and subtracted those two resulting data sets. Because the interfering lines, and wall scattering, are generally not polarization sensitive, most Raman and Rayleigh lines remain.

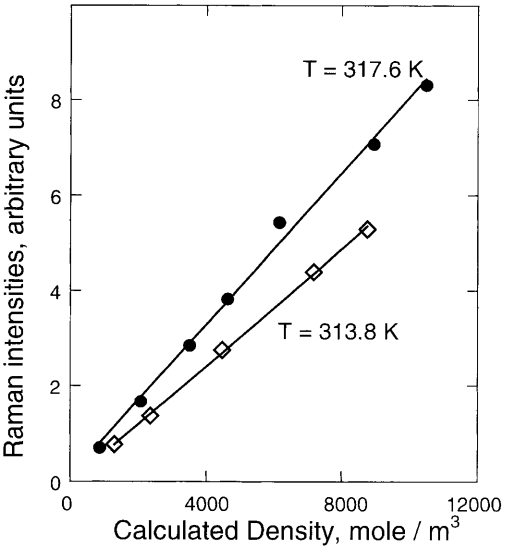

Fig. 5. Plots of scattering intensity vs. molar density of carbon dioxide at 317.6 K, at 313.8 K, and a least-squares linear fit to each. The two slopes were adjusted to be easy to separate visually. The temperatures were greater than the critical temperature, i.e., $T_c = 304.2$ K and our highest pressures (up to 96.8 bar) were greater that the critical pressure, i.e., $P_c = 73.8$ bar. These "normal" data were acquired after the beam bending was eliminated

Knapp et al. [26] constructed a system in which signals from those two polarizations could be acquired simultaneously on a single-shot basis.

We found that repeatability in determining relative cross sections from various species is good, but that agreement with previous investigators is inadequate. That means that calibration is essential: preferably with the calibration material in the same location as the sample to be analyzed. Calibration is probably best done with a mixture, of all desired species, of known composition. Then intensities from all species are simultaneously acquired and the effect of a number of sensitive experimental parameters drops out (for example, shot-to-shot laser energy variations, window fouling, etc.).

Within the precision of our data, *Raman signals are a linear function of gas density*. The best signals are available in high-pressure media. After a calibration for a given experimental setup, quantitative density and temperature diagnostics can be done simply. This is in contrast to LIF or Rayleigh measurements where, as discussed in the introduction, serious problems exist for which calibration is extremely difficult.

Acknowledgements. We thank the National Aeronautics and Space Administration (Grant NAG3-1800) and the Ford Motor Company for financial support. We also thank David Huestis, SRI International, for a helpful conversation that pointed out the history of the O_3 formation from O_2 via KrF irradiation.

References

1. E.W. Rothe, P. Andresen: Appl. Opt. **36**, 3971 (1997)
2. J.W. Daily: Prog. Energy Combust. Sci. **23**, 133 (1997)
3. A.C. Eckbreth: *Laser Diagnostics for Combustion Temperature and Species*, 2nd ed. (Gordon and Breach, Amsterdam 1996) p. 222
4. K. Kohse-Höhinghaus: Prog. Energy Combust. Sci. **20**, 203 (1994)
5. E.W. Rothe, Y. Gu, A. Chryssostomou, P. Andresen, F. Bormann: Appl. Phys. B **66**, 251 (1998)
6. J.W. Daily, E.W. Rothe: Appl. Phys. B **68**, 131 (1999)

7. K.L. McNesby, J.B. Morris: J. Raman Spectrosc. **26**, 487 (1995)
8. M. Ridder, A.A. Suvernev, T. Dreier: J. Chem. Phys. **105**, 3376 (1996)
9. C.H. Wang, R.B. Wright: J. Chem. Phys. **59**, 1706 (1973)
10. A. Hacura: Phys. Lett. A **227**, 237 (1997)
11. D. Fabre, B. Oksengorn: Appl. Spectrosc. **46**, 468 (1992)
12. Y.H. Wu, S. Sasaki, H. Shimizu: J. Raman Spectrosc. **26**, 963 (1995)
13. See, e.g., D.A. Long: *Raman Spectroscopy*, (McGraw Hill, New York 1977)
14. G. Herzberg: *Infrared and Raman Spectra* (Van Nostrand, New York 1945)
15. G. Grünefeld, P. Andresen, H. Schlüter, E.W. Rothe: Appl. Phys. B **62**, 241 (1996)
16. K.M. Gough, W.F. Murphy: J. Chem. Phys. **85**, 4290 (1986)
17. K.M. Gough, W.F. Murphy, T. Stroyer-Hansen, E.N. Svendsen: J. Chem. Phys. **87**, 3341 (1987)
18. J. Martin: J. Raman Spectroc. **18**, 139 (1985)
19. J.H. Dymond, E.B. Smith: *The Virial Coefficients of Pure Gases and Mixtures, a Critical Compilation* (Clarendon Press, Oxford 1980)
20. T.G. Slanger, L.E. Jusinski, G. Black, G.E. Gadd: Science **241**, 945 (1988)
21. D.E. Freeman, K. Yoshino, W.H. Parkinson: Science **250**, 1432 (1990)
22. R. Span, W. Wagner: J. Phys. Chem. Ref. Data **25**,1509 (1996)
23. A. Bideau-Mehu, Y. Guern, R. Abjean, A. Johannin-Gilles: Opt. Commun. **9**, 432 (1973)
24. H.W. Schrötter, H.W. Klöckner: In *Raman Spectroscopy of Gases and Liquids* ed. by A. Weber (Springer, Berlin, Heidelberg 1979)
25. G. Grünefeld, V. Beushausen, P. Andresen: Appl. Phys. B **61**, 473 (1995)
26. M. Knapp, A. Luczak, V. Beushausen, W. Hentschel, P. Mantz, P. Andresen: In Twenty-sixth Symposium (International) on Combustion/The Combustion Institute (Naples, July 28 to August 2, 1996) pp. 2589–2596